UNIVERSITY of York

This is a repository copy of *Modeling Sparsely Reflecting Outdoor Acoustic Scenes using the Waveguide Web*.

White Rose Research Online URL for this paper:
https://eprints.whiterose.ac.uk/115692/

Version: Accepted Version

Article:

White Rose
university consortium
Universities of Leeds, Sheffield & York

eprints@whiterose.ac.uk
https://eprints.whiterose.ac.uk/

Modeling Sparsely Reflecting Outdoor Acoustic Scenes using the Waveguide Web

Francis Stevens, Damian T Murphy, Lauri Savioja, *Senior Member, IEEE*, and Vesa Välimäki, *Fellow, IEEE*

Abstract—Computer games and virtual reality require digital reverberation algorithms, which can simulate a broad range of acoustic spaces, including locations in the open air. Additionally, the detailed simulation of environmental sound is an area of significant interest due to the propagation of noise pollution over distances and its related impact on well-being, particularly in urban spaces. This paper introduces the waveguide web digital reverberator design for modeling the acoustics of sparsely reflecting outdoor environments; a design that is, in part, an extension of the scattering delay network reverberator. The design of the algorithm is based on a set of digital waveguides connected by scattering junctions at nodes that represent the reflection points of the environment under study. The structure of the proposed reverberator allows for accurate reproduction of reflections between discrete reflection points. Approximation errors are caused when the assumption of point-like nodes does not hold true. Three example cases are presented comparing waveguide web simulated impulse responses for a traditional shoebox room, a forest scenario and an urban courtyard, with impulse responses created using other simulation methods or from real world measurements. The waveguide web algorithm can better enable the acoustic simulation of outdoor spaces and so contribute towards sound design for virtual reality applications, gaming and auralisation, with a particular focus on acoustic design for the urban environment.

Index Terms—Acoustics, acoustic propagation, acoustic signal processing, IIR digital filters, numerical simulation.

I. Introduction

ARTIFICIAL reverberation research has, until recently, striven mainly for the realistic imitation of rooms, concert halls, and other indoor acoustic spaces [1], [2]. For this purpose, there are several specialized modeling techniques, such as the ray-tracing [3], image-source [4], [5], digital waveguide [6], [7], feedback delay networks (FDNs) [8]–[10], and finite-difference time-domain (FDTD) [11]–[14] methods. However, there has been relatively little research looking at modeling of sparsely reflecting outdoor acoustic scenes, although environmental sound is of significant importance, particularly because of the propagation of noise pollution over distances and its impact on human health and well-being [15]. This paper proposes a new modeling technique for reverberant

open acoustic environments, considering both forests and urban scenes. Such spaces are important for wider study in relation to how green infrastructure (e.g. trees and other similar natural interventions) and architectural design might have a positive impact on the soundscape of urban areas [16], [17], as well as in more creative applications such as sound design for film soundtracks and interactive computer games [18].

Early research contributions have considered the acoustic properties of outdoor environments, such as streets [19] and forests [20], both of which have a special character that contributes to the sonic experience a person has of these particular locations. For instance, in [21] it was shown that acoustic scattering from the tree trunk is a key factor affecting the behavior of mid-frequency attenuation for sound propagation through trees. Surprisingly, a bamboo forest has good acoustic characteristics for certain types of music [22] and outdoor acoustics also have a connection to concert halls, as shown in a study by Lokki et al. who demonstrated that the finite difference time domain (FDTD) technique is suitable for modeling the acoustics of ancient amphitheaters, which are open but can have excellent acoustic properties [23]. A related study, that considered the acoustic characteristics of an historic street, combined impulse response measurement of the existing site and geometric acoustic modeling of the historic environment as part of an analysis of its suitability for dramatic performances [24].

Recent research has shown a growing interest in the modeling of urban environments. Kang modelled the acoustics of a town square using image-source and radiosity methods to predict the sound pressure level [25]. Collecchia et al. studied the acoustic characteristics of narrow alleyways and simulated their interesting behavior using the image-source method [26]. Recently, Stienen and Vorländer demonstrated how to auralize the propagation of traffic noise in an urban environment [27]. An outdoor urban environment was also at the centre of a study that explored how spatial impulse response measurement, and reflection analysis can be used to help determine source localisation [28], [29].

Some researchers have also been interested in modeling natural environments, such as those containing forests and hills, which strongly reflect sound. Pieren and Wunderli [30] have studied how cliffs in an Alpine valley reflect noise and have proposed a model to account for this phenomenon in sound propagation calculations. Shelley et al. measured forest acoustics in a distant location in Finland, both in the summer and in the winter, to provide impulse responses for convolution-based reverberation [31]. In [32], recorded sound scenes were combined with modelled soundscape interventions, in this case,

a FDTD simulation of a sonic crystal noise barrier, and used as part of a virtual soundwalk perceptual evaluation in order to elicit the effectiveness of applying such design strategies.

Spratt and Abel have proposed a general waveguide method called *Treeverb* for modeling the acoustics formed by trees in a forest [33]. Their model can be interpreted to be 2.5-dimensional, as it describes the geometry, including the locations of the source, trees, and the receiver, on a plane, and the structure is then extended in the third dimension. However, as more trees are added into the model, it quickly becomes too large for efficient computation, in terms of both number of operations and memory use, so Spratt and Abel chose to implement an image-source version of their method for faster simulation [33].

Another example digital reverberator representing an extension of the waveguide method is the scattering delay network (SDN) [18], [34], a method conceptually similar to the feedback delay network (FDN) [8] that consists of a set of discrete nodes representing the reflection points of a given environment connected by a set of waveguides.

This work extends the Treeverb model by formulating a novel type of waveguide network [6], [7] called a *Waveguide Web* (WGW). Like the SDN, a WGW is a network of discrete nodes, including, source, receiver and a number of reflection points, which can be, for example, trees or other reflective surfaces. The WGW differs distinctly from the digital waveguide mesh, which is a regular grid structure of scattering nodes and interconnections, used for modeling multidimensional wave propagation, also usually in closed systems [35]–[38]. This paper shows that the proposed WGW has similarities to, but is also different from, the recently introduced scattering delay network (SDN) approach to reverberation design as it extends the design of the SDN to incorporate directionally-dependent filtering at the node positions.

This paper is organized as follows. Section II gives a brief overview of the Treeverb and SDN methods, which are those closest to the proposed WGW method. Section III introduces the theory of the WGW model. Section IV presents the evaluation of the method by way of three case studies: the acoustic simulation of a shoebox room, a forest-like environment, and an urban courtyard. Section V concludes this paper.

II. BACKGROUND

A. Treeverb

Although the acoustics of forests have been studied previously (e.g. [20], [22]), to date, as cited in [1], only one study has attempted to simulate this reverberant effect. Spratt and Abel's *Treeverb* is a digital reverberator designed to model the scattering of acoustic waves between a number of trees as might be found in a forest environment [33].

In this work, the forest environment is considered as a two-dimensional geometry, with defined source and receiver locations, and a random arrangement of trees. This establishes a fixed network of connected paths between each node, defined as either source, receiver or tree. Each path is modelled using a time delay and attenuation factor, or spreading loss, in much
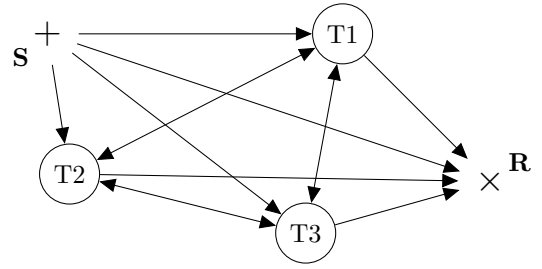

Fig. 1. A simple *Treeverb*, or digital waveguide, network topology for modeling forest acoustics, consisting of three tree-nodes, T1, T2, T3, and a single source, S, and receiver R. The tree-nodes are connected via bidirectional delay lines, with the source and receiver connected to these tree-nodes via unidirectional delay lines. Each delay line has an attenuation factor associated with it and directional dependent filtering and scattering takes place at each tree-node connection. After [33].
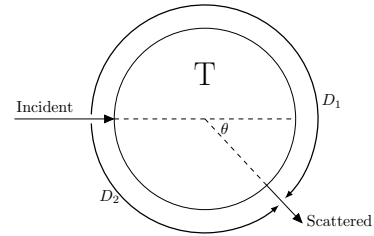

Fig. 2. An acoustic wave incident on a tree trunk T, represented as a rigid cylinder, and the resultant scattered wave at angle θ as formed by the two paths, D_1 and D_2, around the tree. After [33].

the same way as in other reverberation algorithms. However, in this case boundary reflections are better considered as tree-node interactions, where a tree is modelled as a rigid cylinder. Signals incident on a tree-node are scattered in a frequency dependent manner, with appropriate proportions of the incident signal being transmitted to other connected nodes (either receiver or tree), or reflected and returned along the path of the incident signal. Hence Treeverb can be considered as a closed network of lossless *bidirectional waveguides* connected via tree-node *scattering junctions* with attenuation losses also lumped at these discrete points in the network, and so belongs to the *digital waveguide network* family of digital reverberators, first proposed in [6] and developed further in [7]. A simple example network is shown in Fig. 1 consisting of three interconnected tree-nodes, T1, T2, T3, and a single source, S, and receiver, R. The tree-nodes are connected via bidirectional delay lines, with the source and receiver connected to these tree-nodes via unidirectional delay lines. Each delay line has associated with it a distance dependent attenuation factor.

Scattering at a tree-node interaction point takes place in a frequency dependent manner, based on Morse's solution to the acoustic scattering from a rigid cylinder [39]. In [33] an approximation of this solution is used to model the scattering occurring at each tree. In this, a plane wave incident on a rigid cylinder produces a result formed of two parts, defined by movement of the acoustic wave both clockwise and anti-clockwise around the cylinder.

Figure 2 demonstrates this effect where the scattered wave of interest is at an angle θ, with respect to the angle of incidence,
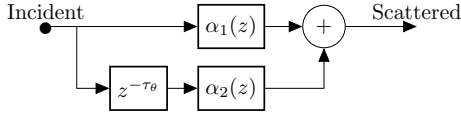
Fig. 3. A block diagram of the tree-node scattering filter defined according to τ_θ, the angle dependent delay in samples. After [33].

due to interaction with a rigid cylindrical tree trunk, T, with radius, r. The two path lengths around T are defined as D_1 (clockwise) and D_2 (anticlockwise) and hence the path length difference $D_\theta = 2r\theta$, or, for a given sampling rate $1/f_s$, $\tau_\theta = 2r\theta f_s/c$ where c is the speed of sound and τ_θ is the angle dependent delay in samples.

The signal to arrive first has a high-pass characteristic for all scattering angles. The second signal has a high-pass characteristic for small scattering angles, where the wave essentially passes straight through the cylinder, and a low-pass characteristic for large (and hence back) scattering angles.

Fig. 3 expresses the required angle dependent scattering filter in block diagram form as used in [33]. $z^{-\tau_\theta}$ is the sample delay equivalent to the path distance between the two parts of the scattered signal, $\alpha_1(z)$ represents the filtering action associated with the shorter of the two scattering paths, and $\alpha_2(z)$ represents the filtering associated with the longer path.

As stated in Section I, this two-dimensional Treeverb network geometry definition is essentially 2.5-dimensional, and both spherical spreading losses, assuming a perfectly absorbing forest floor, and cylindrical spreading losses can be considered, resulting in different, if non-physical in the latter case, reverberant effects. Although Treeverb was conceptually derived as a digital waveguide network, computational limits in terms of both run-time costs and memory requirements resulted in an implementation based on the geometrical acoustics image-source method instead [5]. This implementation creates an offline impulse response as the system output for use as part of a convolution based reverberation algorithm.

B. Scattering Delay Networks

Another digital waveguide network based digital reverberator design is the scattering delay network (SDN) [18], [34]. An SDN reverberator is similar to the Treeverb system in that it decomposes the space to be modeled into a set of nodes representing the first-order reflection points, interconnected with bidirectional waveguides. A signal is introduced to the SDN from source node, S, and output at receiver, R, both connected via unidirectional delay lines. In the Treeverb reverberator the tree-nodes make up the whole of the physical surroundings, resulting in a relatively sparse set of possible reflection paths for multiple reflection orders. However, the wall-nodes in a SDN system are accurate for first-order reflections but only approximate acoustic behaviour at higher orders as the much larger surfaces involved and typically closed nature of the system result in many more possible connected paths.

A block diagram representing the operation of the SDN reverberator is shown in Fig. 4 after [34] where a detailed description of each stage can be found and is presented here in

overview. The input signal, $x(n)$, is applied at the source node, and through the application of input delay and attenuation matrix operators ($\mathbf{D}_s(z)$ and $\mathbf{G}_s$ respectively), this signal is transmitted to each wall-node. The scattering matrix $\bar{\mathbf{S}}$ is then applied to scatter this incoming signal between wall-nodes with $\mathbf{H}(z)$ applying frequency dependent absorption at each.

For higher than first-order reflections, a feedback loop comprising inter-node delays $\mathbf{D}_f(z)$ in series with permutation matrix $\mathbf{P}$ is applied to recursively model the higher order reflection behavior of the system. Attenuation matrix $\mathbf{G}_r$ and delay factors $\mathbf{D}_r(z)$ associated with each wall-node to receiver connection are then applied for generating output signal $y(n)$. The matrices γ_s and γ_r represent the directivity patterns between the SDN nodes and the source and receiver respectively. Note that for all of the simulations included here the source and receiver are modelled as omnidirectional, so neither γ_s nor γ_r will be considered further. Finally, $z^{-D_{sr}}$ and g_{sr} represent the direct path delay and attenuation respectively,

Of particular interest are the scattering matrix $\bar{\mathbf{S}}$ and permutation matrix $\mathbf{P}$. The former represents the scattering associated with the SDN system as a whole, and is formed of identical smaller scattering matrices, $\mathbf{S}$, representing the scattering at each individual wall-node:

$$\mathbf{S} = \frac{2}{N-1}\mathbf{1}_{(N-1)(N-1)} - \mathbf{I} \qquad (1)$$

where N is the number of wall-nodes in the system, $\mathbf{1}$ is a matrix of ones, and $\mathbf{I}$ is an identity matrix. For outgoing wave pressure signal p_{ij}^- and incoming wave pressure p_{ij}^+ from wall-node i to wall-node, j, $\mathbf{S}$ determines the outgoing pressure signal from one wall-node to the other wall-nodes in the system given knowledge of the incoming pressure signal:

$$p_{ij}^- = \mathbf{S}p_{ij}^+ \qquad (2)$$

This can be extended to characterise the whole system $\bar{\mathbf{S}}$:

$$\bar{\mathbf{S}} = \mathrm{diag}(\underbrace{\mathbf{S}\ldots\mathbf{S}}_{N}) \qquad (3)$$

The scattering matrix $\bar{\mathbf{S}}$ is therefore a $N(N-1) \times N(N-1)$ matrix that determines the spread of acoustic energy among the bidirectional delay lines connecting the wall-nodes. For the system to work recursively and model higher order reflection paths it is required to re-arrange the result of this scattering in the feedback loop ready for input and a new scattering operation. Note that, after scattering, the outgoing pressure value p_{ij}^- is equivalent to the incoming pressure values p_{ij}^+ at the next scattering instance, which, in order to be the correct input to the next scattering operation, must be rearranged to form the vector multiplied by the scattering matrix $\bar{\mathbf{S}}$. Hence the permutation matrix $\mathbf{P}$ is defined to rearrange the elements appropriately.

For an N node SDN, each node has $N-1$ permutation terms. Given wall-node m such that $1 \leq m \leq N$, connected to n other wall-nodes where $1 \leq n \leq N$ and $n \neq m$, we define:

$$P_{m,n} = \begin{cases} m-1+(n-1)(N-1), & n < m \\ mN + (n-m+1)(N-1), & n > m \end{cases} \qquad (4)$$

Such that the required permutation, σ, is given by:

$$\sigma = \begin{pmatrix} 1, & 2, & \ldots, & N-1, & \ldots, & (N-1)(N-1)+1, & \ldots, & N(N-1) \\ P_{1,2}, & P_{1,3}, & \ldots, & P_{1,n}, & \ldots, & P_{m,1}, & \ldots, & P_{m,n-1} \end{pmatrix} \qquad (5)$$
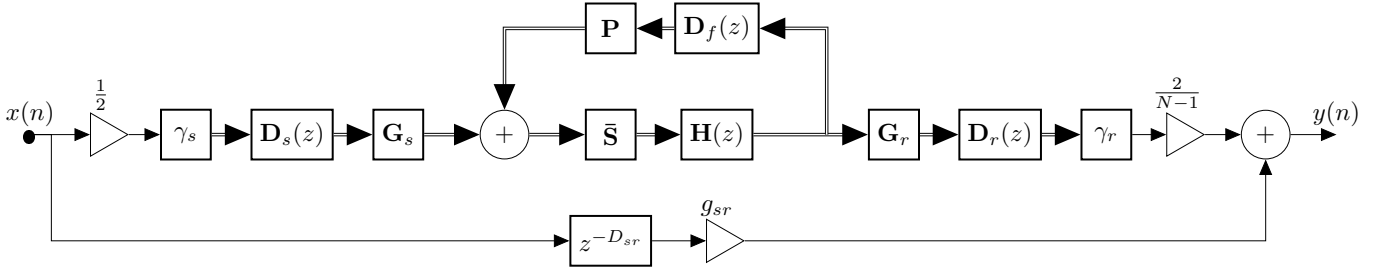
Fig. 4. The scattering delay network overview block diagram, taking account of explicit direct sound and first reflection paths via wall-nodes for a given source and receiver position, with higher order reflections derived via the main feedback loop, after [34].

The input scaling factor of $\frac{1}{2}$ is included in order to provide the intended pressure at each node [34]. This input scaling is then compensated for by the output being scaled by a factor of $\frac{2}{N-1}$. The denominator value of $N-1$ in this case compensates for the $N-1$ 'copies' of the input signal being applied to each of the N nodes by the input delay and attenuation matrices, copies which are made to allow the output result of the application of $\mathbf{G}_s$ to be combined with the results of applying the permuation matrix.

The application of $\mathbf{P}$ to the incoming pressure values p_{ij}^+ therefore results in the required input reordering. This alternating scattering-permutation matrix operation allows the SDN to successively model the interaction defined by the bidirectional delay elements connecting the wall-nodes. The SDN is, therefore, an efficient and effective method of reverberation design for room acoustic simulation, with accurate first-order reflections and good perceptual accuracy [34]. However, for correct scattering paths between nodes, to potentially incorporate direction dependent filtering as found when considering reflections from objects similar to a rigid cylinder, a modified approach is required.

III. WAVEGUIDE WEB

This section introduces the WGW, a novel type waveguide network that has been designed to allow for the implementation of directionally dependent filtering at each node. As such it allows for the precise characterization of second-order reflection attenuation, following previous work indicating the importance of first- and second-order reflections in the characterization of the acoustics of sparse outdoor spaces [28].

A. Design Overview

The design of the Waveguide Web is similar to the SDN where the modeled space is represented by a set of scattering nodes connected to one another via bidirectional delay lines. Source and receiver nodes are also connected to these scattering nodes by unidirectional delay lines. Where the WGW differs from the SDN is in the scattering action at each node. Whereas the SDN implementation allows for one filtering action only at each node, the WGW design allows for directionally dependent filtering to be implemented. Like the SDN, the WGW method presents an abstracted representation of a space, based on an interconnected network of significant reflection points. These points can be at any 3D position, as required by the geometry of the system being modeled.

1) WGW Connections: Fig. 5 shows all of the connections and filters associated with a node j in an N-node structure, including the source-to-node connections, inter-node connections, and node-to-receiver connections. In this diagram K is a vector, formed of $N-1$ elements, denoting the indices of all nodes present in the system apart from node j. For example, if $N=4$ and $j=3$, then $K=[1,2,4]$. If the case was that $j=2$ however, then $K=[1,3,4]$.

In the SDN, each node only has a single filter associated with it. As shown in Fig. 5, in the WGW design each node has N^2 filters: one filter for the first-order reflection between source and receiver occurring at that node; $N-1$ filters corresponding to incoming signals from all other nodes and outgoing to the receiver; $N-1$ filters corresponding to the signal incoming from the source and outgoing to all other nodes; and $(N-1)(N-1)$ filters corresponding to recirculating signals incoming from all other nodes and then also outgoing to all other nodes.

The notation for these filters is as follows: H_{ijk} represents a filter at node j acting on a signal arriving from node i that will ultimately be sent to node k. In the case of the signal arriving from the source node, S is used in place of i, and where the signal is ultimately being sent to the receiver node, R is used in place of k.

The delay lines present in Fig. 5 are absorptive, as represented by the lumped gain factors placed at the end of each one. In the case of second order reflections the gain values for the 'middle path' of each one are combined with the attenuation multiplier for the final node to receiver path. In Fig. 5 it is shown that there are three steps in the WGW structure where this attenuation takes place: between the source and each node (g_{Sj} in Fig. 5), between each node and the receiver (g_{jR}), and between each node and the receiver where the incoming signal is from each of the other nodes and not from the source ($g_{K_ijR} \cdots g_{K_{N-1}jR}$).

In order to maintain correct attenuation according to $\frac{1}{r}$, where r is the distance traveled, the delay line attenuation values present at each of the points identified in Fig. 5 are

Fig. 5. Structure of the source-to-node, inter-node, and node-to-receiver connections at a single WGW node. The implementation of the directionally dependent filtering at each node is shown, including how the the elements of the scattering operator **S** are applied to the incoming signal from each node.

calculated using the following equations:

$$g_{ST_M} = \frac{1}{\|x_S - x_{T_M}\|} \tag{6}$$

$$g_{T_M R} = \frac{1}{1 + \frac{\|x_{T_M} - x_R\|}{\|x_S - x_{T_M}\|}} \tag{7}$$

$$g_{T_M T_N R} = \frac{1}{1 + \frac{\|x_{T_N} - x_{T_M}\| + \|x_R - x_{T_N}\|}{\|x_S - x_{T_M}\|}} \tag{8}$$

where g_{ST_M} is the attenuation between the source and the node indicated by T_M, $g_{T_M R}$ is the attenuation between node T_M and the receiver, and $g_{T_M T_N R}$ is the attenuation associated with the total path from node T_M via node T_N to the receiver. Note that (6) and (7) are formulated identically in the SDN [18] to give correctly attenuated first-order reflections. The WGW extends the SDN algorithm in this regard with the addition of (7) providing correctly attenuated second-order reflections. Higher order reflections are reproduced less accurately, and do not follow the $1/r$ law, but still produce a rich reverberation tail. In Fig. 5, the gain quantities defined by (6)-(8) are represented by the multiplication operators labeled g_{Sj}, g_{jR}, and $g_{K_i jR} \ldots g_{K_{N-1} jR}$ respectively.

Also shown in Fig. 5 are the elements of the scattering matrix **S** and how they are applied to incoming signals at each node. In Fig. 5 each multiplier marked $\mathbf{S}_{ij}$ indicates the element in row i and column j of the matrix **S**, as in (1). There is an important distinction here between the WGW and the SDN. In the case of the SDN, the scattering operation is applied to incoming signals at each node regardless of their point of origin and further destination. Here the scattering operator allows for directionally dependent filtering to be applied by

making $N - 1$ copies of each incoming signal and filtering as appropriate.

B. WGW Structure

Presented in Fig. 6 is the overall structure of the WGW in block diagram form. A comparison with Fig. 4 shows the similarity between the designs of the WGW and the SDN as well as their differences. In the case of the WGW the first-order reflections are calculated separately along with the direct path. This is because the filters associated with first-order reflections (i.e. from source-to-receiver via a single tree) are not appropriate to be fed back via scattering and permutation operations. Instead, the main section of the WGW is used to model the second-order reflections represented by the given tree layout, with reflections of third-order and above calculated using the feedback loop.

Starting with the first-order reflection feed-forward path in the block diagram of Fig. 6,

$$\mathbf{D}_S(z) = \text{diag}(z^{-D_{S1}}, z^{-D_{S2}}, \ldots, z^{-D_{SN}}) \tag{9}$$

$$\mathbf{D}_R(z) = \text{diag}(z^{-D_{1R}}, z^{-D_{2R}}, \ldots, z^{-D_{NR}}) \tag{10}$$

are the source and receiver delay matrices for the first-order section.

$$\mathbf{H}_{STR}(z) = \text{diag}(H_{S1R}(z), H_{S2R}(z), \ldots, H_{SNR}(z)) \tag{11}$$

is the $N \times N$ matrix that contains the filters representing the first-order reflections, and $z^{-D_{SR}}$ and g_{SR} are the direct path
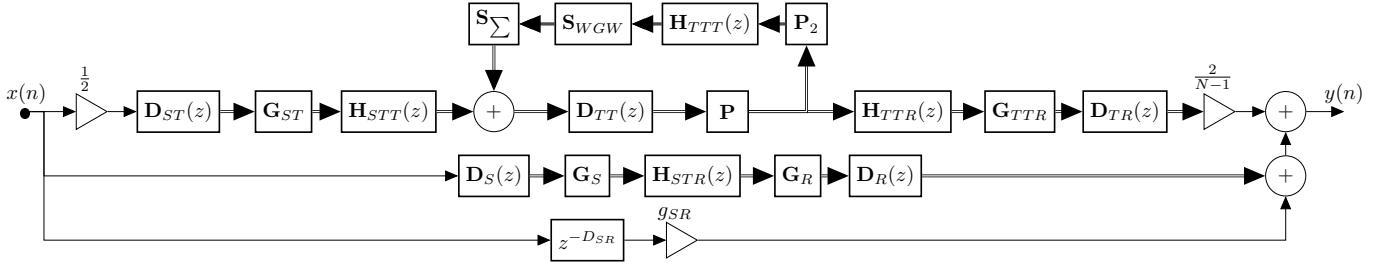
Fig. 6. Block diagram of the WGW reverberator. Here there are paths for the explicit calculation of first-order reflections, alongside the direct sound path, separate from the main path for the calculation of reflections of second-order and above.

delay and attenuation respectively. Considering the second-order reflection feed-forward path in the block diagram of Fig. 6,

$$\mathbf{D}_{ST}(z) = \text{diag}(\underbrace{z^{-D_{S1}}\dots z^{-D_{S1}}}_{N-1}, z^{-D_{S2}}\dots z^{-D_{SN}}) \quad (12)$$

$$\mathbf{D}_{TT}(z) = \text{diag}(\underbrace{z^{-D_{12}}\dots z^{-D_{12}}}_{N-1}, z^{-D_{1N}}\dots z^{-D_{N\,(N-1)}}) \quad (13)$$

$$\mathbf{D}_{TR}(z) = \text{diag}(z^{-D_{2R}},\dots,z^{-D_{NR}},\dots,z^{-D_{1R}},\dots,z^{-D_{(N-1)R}}) \quad (14)$$

are the source-node, inter-node, and node-receiver delay matrices, and

$$\mathbf{H}_{STT}(z) = \text{diag}(H_{S12}(z)\dots H_{S1N}(z),\dots,H_{SN1}(z),\dots,H_{SN(N-1)}(z)) \quad (15)$$

$$\mathbf{H}_{TTR}(z) = \text{diag}(H_{12R}(z),\dots,H_{1NR}(z),\dots,H_{N1R}(z),\dots,H_{N(N-1)R}(z)) \quad (16)$$

are the source-node-node, node-node-receiver filter matrices. Note that these filters also include the effect of absorption at a node due to the process of reflection.

$$\mathbf{G}_{ST} = \text{diag}(\underbrace{g_{S1}\dots g_{S1}}_{N-1}, g_{S2}\dots g_{SN}) \quad (17)$$

$$\mathbf{G}_{TTR} = \text{diag}(g_{12R},\dots,g_{1NR},\dots,g_{N1R},\dots,g_{N(N-1)R}) \quad (18)$$

are the second-order source-node and node-receiver attenuation matrices respectively, and

$$\mathbf{G}_S = \text{diag}(g_{S1}, g_{S2},\dots,g_{SN}) \quad (19)$$

$$\mathbf{G}_R = \text{diag}(g_{1R}, g_{2R},\dots,g_{NR}) \quad (20)$$

are the source and receiver attenuation matrices for the first-order section. The permutation matrix $\mathbf{P}$ is formulated according to the SDN design as described in Section II-B.

C. Feedback Loop

Besides the feedback path, there are $N(N-1)$ channels used in the calculation of second-order reflection paths. In order to accommodate directional dependent filtering at each node $N-1$ copies of each channel must be made. This action is in effect performed by the matrix $\mathbf{P}_2$, creating $N-1$ copies of the output from $\mathbf{P}$.

In order to do this $\mathbf{P}_2$ must take the form of an $N(N-1)(N-1) \times N(N-1)$ matrix. $\mathbf{P}_2$ is formed of multiple copies of a sub-matrix $\mathbf{P}_{2s}$ given by:

$$\mathbf{P}_{2s} = [\underbrace{\mathbf{I}_{N-1}\dots\mathbf{I}_{N-1}}_{N-1}]^T \quad (21)$$

$\mathbf{P}_{2s}$ is then an $(N-1)(N-1) \times (N-1)$ matrix. If we then apply the following tensor product operation (as denoted by $\otimes$):

$$\mathbf{P}_2 = \mathbf{I}_N \otimes \mathbf{P}_{2s} \quad (22)$$

we get the desired $N(N-1)(N-1) \times N(N-1)$ matrix $\mathbf{P}_2$. The result of applying $\mathbf{P}_2$ can then be input to $\mathbf{H}_{TTT}(z)$, which is formulated according to

$$\mathbf{H}_{TTT}(z) = \text{diag}(H_{212}(z),\dots,H_{N1N}(z),\dots,H_{1N1}(z),\dots,H_{(N-1)N(N-1)}(z)) \quad (23)$$

and represents the $N(N-1)(N-1) \times N(N-1)(N-1)$ node-node-node filters.

Following the application of the directionally dependent filtering, the scattering operation can take place. $\mathbf{S}_{WGW}$ is given by:

$$\mathbf{S}_{WGW} = \text{diag}(\underbrace{\text{vec}(\mathbf{S})^T \dots \text{vec}(\mathbf{S})^T}_{N}) \quad (24)$$

and allows for the correct element of $\mathbf{S}$ to be applied to each incoming filter signal. The result must then be summed appropriately to give the total scattering output at each node, using the operator $\mathbf{S}_{\sum}$:

$$\mathbf{S}_{\sum} = \mathbf{I}_{N(N-1)} \otimes [\underbrace{1\dots1}_{N-1}] \quad (25)$$

In this way, the application of both $\mathbf{S}_{WGW}$ and $\mathbf{S}_{\sum}$ recombines the $N(N-1)(N-1)$ channels present in the feedback loop back into the $N(N-1)$ inter-node wave variables required for reinsertion and further propagation through the system.

Since the WGW makes use of essentially the same scattering operation as the SDN, it is similarly stable [10] regardless of the length of the delay lines connecting the nodes. As a result the addition of losses at the nodes will always result in a stable network.

This section has detailed the design and structure of the WGW. Highlighted are the key points where its design differs from that of the SDN, namely: the separate calculation of first-order reflections as well as the direct path; the extension of the structure at each node to accommodate directionally

dependent filtering; and the accordant changes made to the scattering operation.

IV. EVALUATION

This section includes three case studies for evaluating the performance of the WGW:

- A comparison of IR simulations for a shoebox room using the SDN and the WGW. The purpose of this comparison is to validate the WGW and see where the differences in design between the two manifest themselves in the resultant rendered impulse responses.
- A simulation of a forest environment using filters designed according to Spratt and Abel's Treeverb design [33] and Morse's solution to acoustic scattering from a rigid cylinder [39]. The forest environment used is formed of 25 trees arranged in a semi-regular grid pattern. It is evaluated with reference to Chobeau's results regarding the sound propagation in forests [40], and Wiens' MATLAB implementation of Treeverb [41].
- A simulation of an urban courtyard where impulse responses have been previously measured [28], [29]. These measurements were used to inform the structure of the WGW model as an approximation of the space, and to compare with the resultant simulated impulse response.

All of the IRs generated using the WGW here were calculated at a sample rate of 48 kHz, and have been made available online as part of the OpenAIR Library [42].

A. SDN Shoebox Comparison

In order to validate the design of the WGW, presented here is a comparison of a simulation for a $9\,\mathrm{m} \times 7\,\mathrm{m} \times 4\,\mathrm{m}$ shoebox room (with an absorption coefficient $\alpha = 0.2$ defined for all surfaces) made using the SDN [18], and the same simulation made using the WGW. Fig. 7 (a) shows the two results overlaid on one another (with the WGW results marked in red), and Fig. 7 (b) shows the remainder following subtraction of the WGW result from that of the SDN.

The results presented in Fig. 7 validate the design of the WGW as they indicate identical reproduction of the direct sound path and first-order reflections (i.e. at those sample instances the difference between the SDN and WGW simulations is 0). This figure shows the difference in second-order reflection amplitude between the WGW and SDN results, where the WGW calculates them correctly according the the $\frac{1}{r}$ law. This difference is second-order reflection amplitude accordingly leads to further small differences for the reflections beyond the second-order, and as such the reverberant tail of the response. These results can also be validated with reference to Fig. 8 which shows reverberation time for octave bands from 125 Hz to 16 kHz, based on derivation of the T30 room acoustic parameter [43], [44].

The results shown in Fig. 7 and Fig. 8 validate the WGW results as they are close to those obtained from the SDN, but differ according to the novel design elements implemented in the WGW (i.e. the attenuation values given by (6)-(8)). The results shown in Fig. 8 are clearly similar, and fall within the 30% just-noticeable-difference (JND) associated with T30
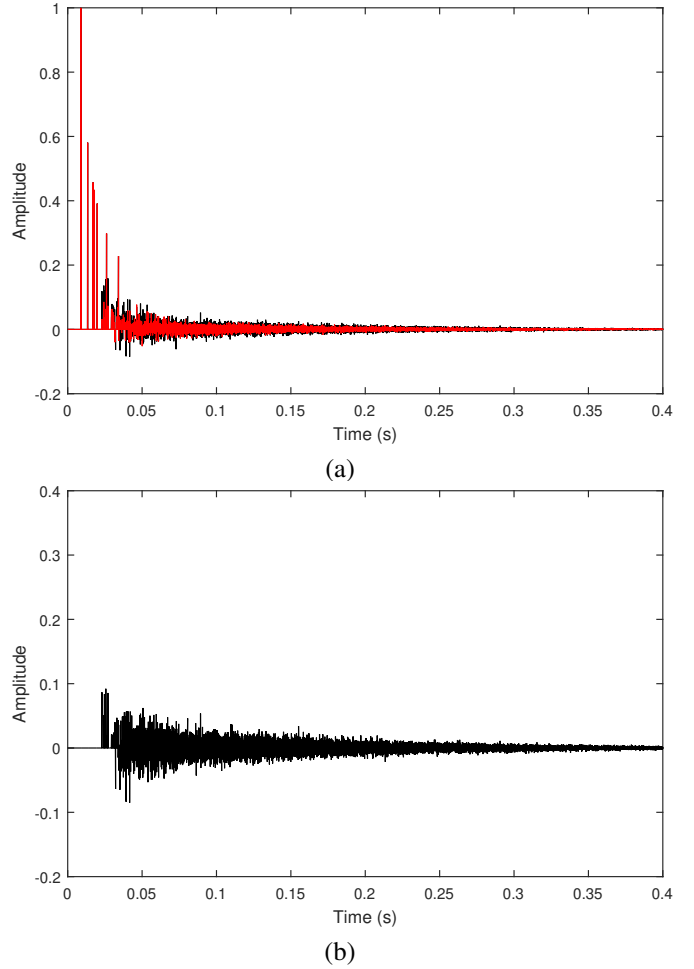

Fig. 7. (a) Comparison of SDN result (black) with WGW (red). (b) Difference between the two.
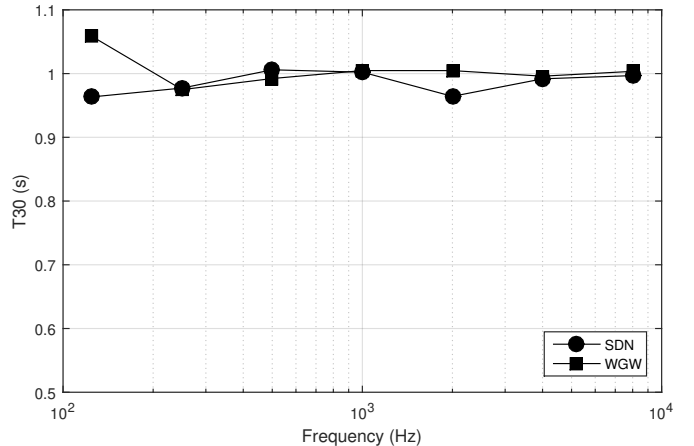

Fig. 8. Octave band reverberation time results for SDN and WGW derived impulse responses obtained from a $9\,\mathrm{m} \times 7\,\mathrm{m} \times 4\,\mathrm{m}$ shoebox-like room simulation.

measurement [45], indicating the results from the SDN and the WGW to be perceptually alike. On this basis the WGW can be used to obtain simulation results for further case studies.

B. Forest Environment

This section includes a comparison of results from the WGW with those from two previous studies regarding the acoustic properties of forest environments: Spratt and Abel's Treeverb design as mentioned in Section II-A; and Chobeau's modeling of forest environments using the transmission line matrix (TLM) method [40].

Chobeau's work was chosen for comparison as its results contain a set of impulse responses based on two-dimensional reflection and scattering from regular arrays of tree positions. This method therefore represents approximate acoustic model of a forest that is suitable for comparison with results gathered from the WGW.

1) Filter Design: As suggested by Spratt and Abel [33], the filtering used at each node when simulating a forest acoustic is designed to emulate scattering from a rigid cylinder (representing a tree trunk). As detailed in Section II-A when a plane wave is incident upon such a cylinder the result is formed of two parts, with scattered propagation paths traveling in each direction around the cylinder.

In Fig. 3, $z^{-\tau_\theta}$ represents a delay equivalent to the path distance between the two parts of the scattered signal, $\alpha_1(z)$ represents the filtering action associated with the shorter of the two scattering paths, and $\alpha_2(z)$ represents the filtering associated with the longer path.

In the current design of the WGW, these filters are implemented using first-order IIR filters that can be used to perform both high and low pass operations. Two of these filters are used in the configuration shown in Fig. 3 to emulate the two scattered paths shown in Fig. 2. A high pass filter is applied to the shorter of the two scattering paths with cut-off frequency f_c defined by:

$$f_c = \frac{c}{(\pi + \theta)r} \tag{26}$$

where f_c has a wavelength equal to the total length of the longer scattering path around the tree. For small scattering angles the longer of the two paths has a high pass characteristic with the same break frequency. For large scattering angles it changes to a low pass filter with cut-off frequency:

$$f_c = \frac{c}{r \cdot \frac{\theta}{\pi}} \tag{27}$$

where f_c has a wavelength equal to the proportion of half of the tree's circumference represented by the scattering angle.

This filtering is applied at each tree node together with the additional application of a reflectance factor determined by the total amount of scattered energy according to Morse's solution. Fig. 9 shows how the total scattered energy changes with the scattering angle. At $\theta = 0$ there is effectively complete transmission, but at $\theta = \pi$ the reflectance value is reduced to about 0.25. This represents an average tree trunk with radius $r = 0.2\,\text{m}$, and is representative of values of r between 0.1 and 0.5 m.

Fig. 10 compares Morse's solution to acoustic scattering from a rigid cylinder with results made using the design detailed here at three different scattering angles. These plots indicate a good match at high frequencies with greater discrepancies appearing
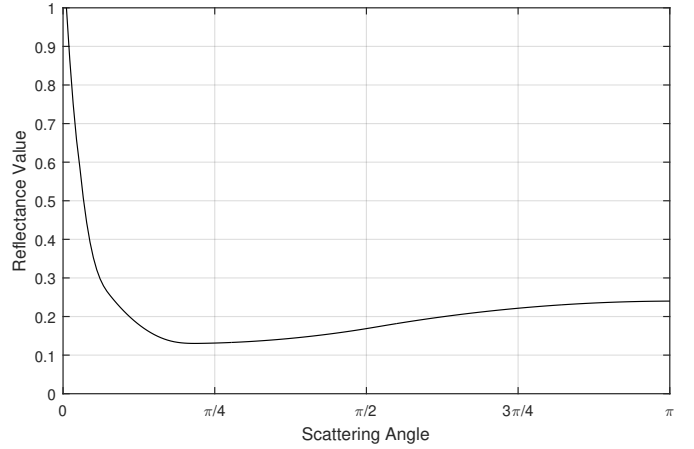
Fig. 9. Plot of reflectance against scattering angle as used in the forest reverb example. These values are generated using Morse's solution to scattering from a rigid cylinder.

at lower frequencies below around 100 Hz. Whilst more sophisticated (i.e. higher order) filters could be implemented to match more closely Morse's solution, the results presented in Fig. 10 are sufficient for use here.

2) Treeverb Comparison: In order to compare WGW results with those made using Treeverb, a MATLAB implementation of the image-source based Treeverb algorithm [41] was used to generate a forest environment (shown in Fig. 11 where 25 trees with radii between 0.2 m and 0.5 m have been distributed over a 30×30 m region. This layout of trees was input to this algorithm and used to generate the IR shown in Fig. 12, as obtained when considering up to fifth-order scattering paths.

This same tree layout is also used to generate the WGW IR shown in Fig. 13. Fig. 14 shows the same IR with a focus on the first 200 ms. Comparison with the Treeverb result shows this to be more plausible with distinct initial reflections followed by a much less reverberant tail.

The lack of more objective analysis of the results obtained in the Treeverb paper make more detailed comparisons somewhat difficult to make. As such, in the next section results made using the WGW method will be compared with results from Chobeau's use of the Transmission Line Matrix (TLM) method to simulate a forest acoustic.

3) Chobeau Comparison: Chobeau made use of multiple forest layouts to determine the effect that tree placement has on sound attenuation level. In Chobeau's thesis it was determined that a major factor affecting the acoustic properties of a forest environment is the filling fraction, i.e. the fraction of the space occupied by the trees (represented by cylinders). For an aligned square grid of cylinders the filling fraction F is given by:

$$F = \frac{\pi d^2}{4a^2} \tag{28}$$

where d is the diameter of the cylinders and a is the 'lattice constant', or the distance between the cylinders' central points [46]. The filling fraction has an affect on the bandwidth of the spectral gaps produced by the environment. According to
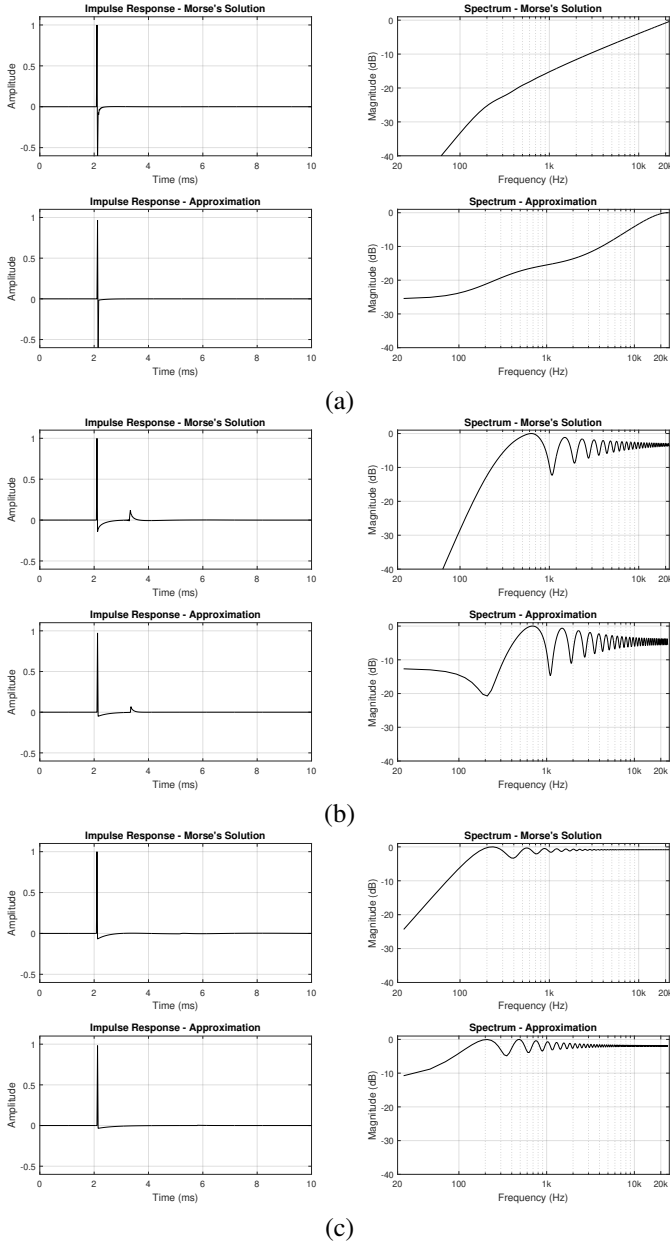
Fig. 10. A comparison of Morse's solution to acoustic scattering from a rigid cylinder with the approximation formed of first-order filters as used in the WGW. For all examples $r = 0.2\,\text{m}$, the three examples represent the following reflection angles: (a) $\theta = 0°$ (b) $\theta = 60°$ (c) $\theta = 180°$.
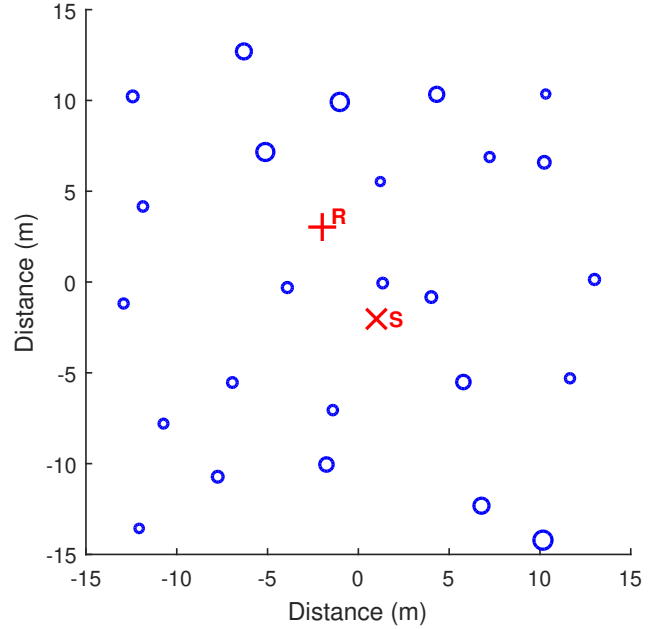

Fig. 11. Forest configuration formed of 25 trees with radii between 0.2-0.5m, one source, S, and one receiver, R, distributed over a $30 \times 30\text{m}$ region, used to generate the impulse response shown in Fig. 5.
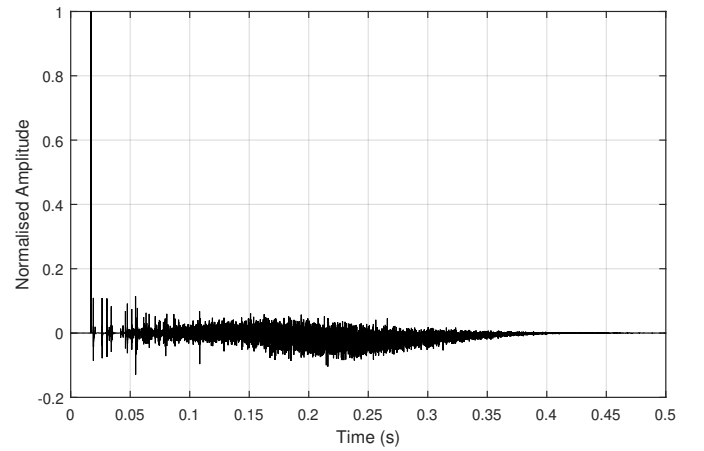

Fig. 12. Impulse response for the forest configuration shown in Fig. 11 generated using Spratt and Abel's Treeverb methodology based on the MATLAB implementation presented in [41].

Bragg's law, the centre frequency of such a band gap can be approximated using:

$$f_c = \frac{c}{2 \cdot a} \tag{29}$$

where c is the speed of sound in air and a is, again, the lattice constant [47].

The three distributions used to generate WGW results are shown in Fig. 15, and were chosen to emulate the different distributions used by Chobeau. For all distributions the trees have a radius of 0.2m. In D1 the lattice constant is 1.42m, for D2 it is 2m, and for D3 it is 1m. The filling fractions for these distributions therefore range from about $F = 0.15$ to about $F = 0.03$.

Using (29), for each of the regular distributions presented here, the centre frequency of an expected band gap can be calculated: for D1, $f_c = 121\,\text{Hz}$; for D2, $f_c = 86\,\text{Hz}$; for D3, $f_c = 172\,\text{Hz}$. These band gaps would typically be expected to be observed in topologies with filling fraction $0.4 < F < 0.6$ [48]. However, one would still expect to see pseudo-bands gaps for low filling fractions [40] corresponding to the distributions used in this paper. Fig. 16 shows a spectral comparison between results for these four distributions.

The results shown in Fig. 16 do line-up with these predictions somewhat, in that the first dip in each spectra for each distribution is near its predicted f_c value. As predicted, however, the low filling fraction associated with the distributions used
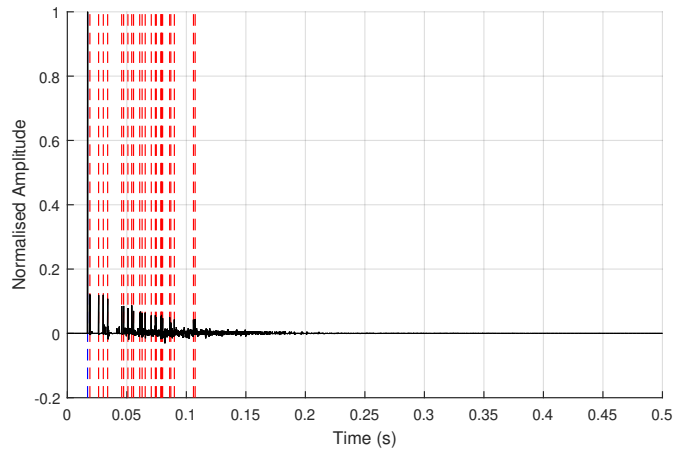
Fig. 13. An IR generated using the WGW for the forest layout shown in Fig. 11. The red lines indicate the timing of first-order reflections.
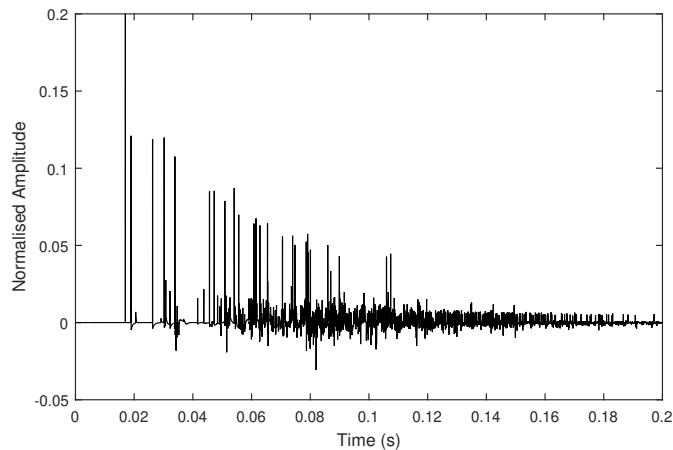

Fig. 14. A closer view of the first 200 ms of the IR shown in Fig. 13.
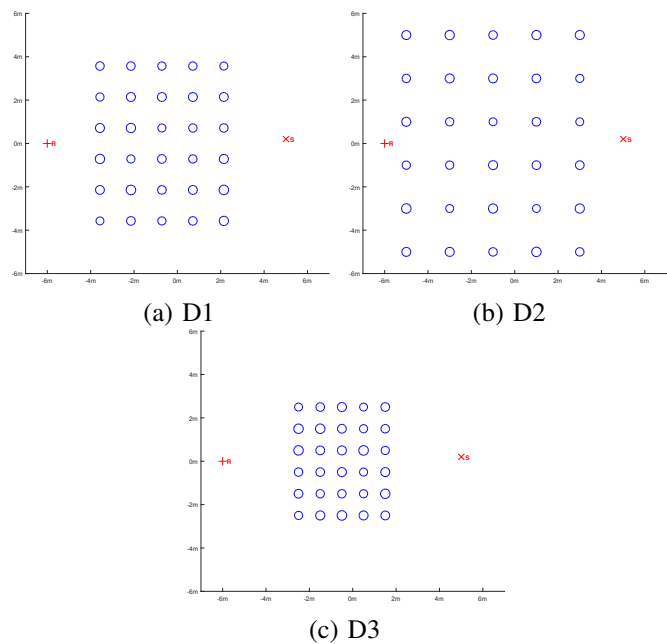

(a) D1

(b) D2

(c) D3

Fig. 15. Schematics of the three distributions used in the forest simulations, each with 30 'trees' of radius $r = 0.2$ m: (a) D1 aligned distribution with 1.42 m spacing; (b) D2 Aligned distribution with 2 m spacing; (c) D3 aligned distribution with 1 m spacing.
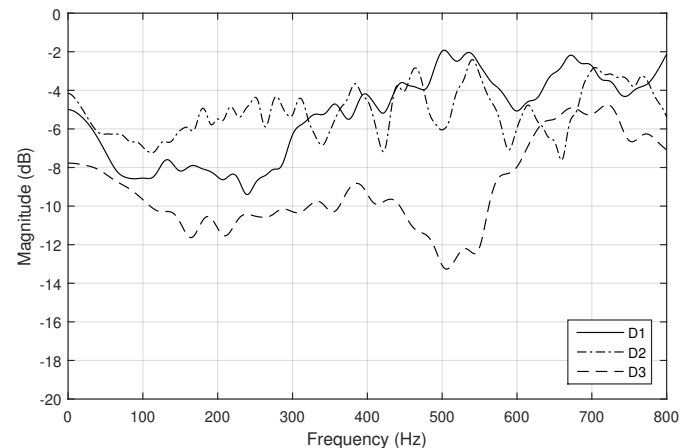

Fig. 16. Frequency responses of simulations made using the three distributions shown in Fig. 15.

means that these spectral band gaps are not very prominent. This is in accord with Chobeau's key findings, where no pronounced band-gaps were observed in simulations of similar forest environments.

Also in accord with Chobeau's results are the global attenuation levels associated with each of the three distributions (-7.57 dB for D1, -6.8 dB for D2, -10.1 dB for D3), where the greatest attenuation is associated with the distributions showing the highest filling fraction. These attenuation levels are calculated as the average of the calculated sound level across all frequencies relative to an environment where no trees are present. The absolute values of these attenuation values are less important than how they relate to one another: they show that attenuation increases with the density of the distribution (i.e. the filling fraction), which is one of two main factors identified by Chobeau as having an effect on attenuation levels.

C. Urban Courtyard

While the WGW's design lends itself to the simulation of a forest acoustic, it is also intended for the modeling of more general sparse outdoor spaces. This section presents a comparison of results with sparsely reflecting IRs as obtained from acoustic measurements in a semi-enclosed courtyard [28]. The node positioning is determined from a full 3D model (shown in Fig. 17) used to calculate the main reflection paths based on a geometrical acoustics approach [29], with nodes placed at a selection of identified main first- and second-order reflection points. The resultant node layout is shown in Fig. 18.

Initial simulations were made using acoustic absorption coefficient (α) values for the materials observed in the internal courtyard buildings (predominately brick) with no filtering applied at each node (due to the relatively minimal frequency dependence in the acoustic absorption coefficients for these
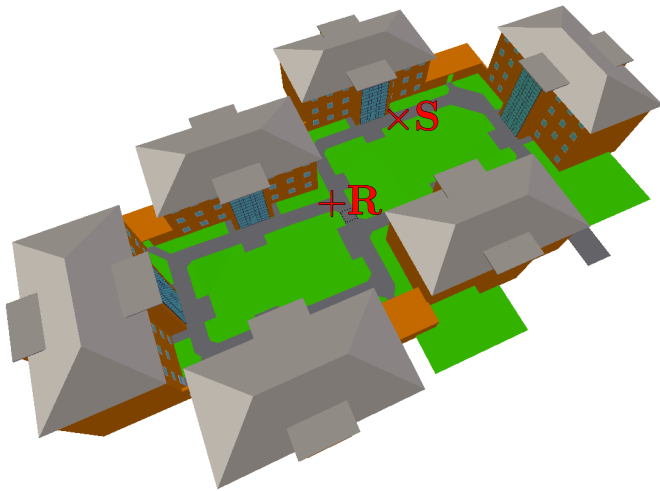
Fig. 17. The 3D model of the urban courtyard considered here, based on actual measurements, and also used to identify the main reflecting surfaces. The labels S and R denote the position of the source and the receiver respectively.
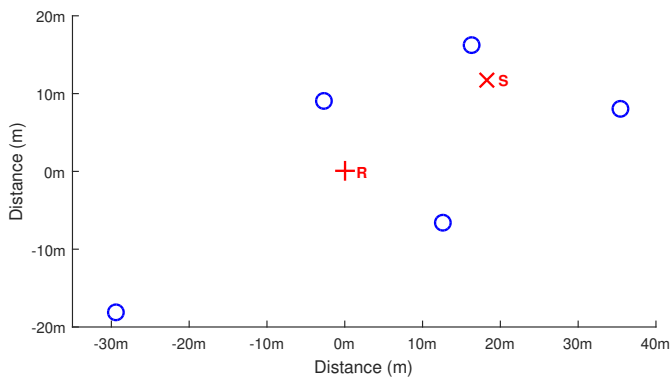

Fig. 18. WGW node layout used for the simulations of the urban courtyard, corresponding to the main reflecting surfaces in Fig 17.
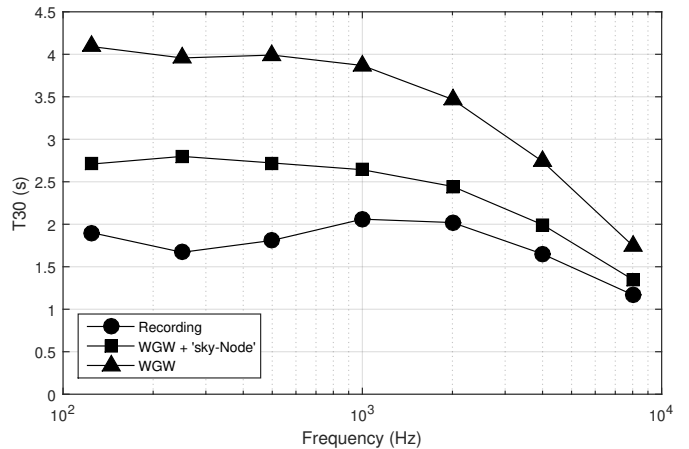

Fig. 19. Octave band reverberation time results for the IR measurement/recording obtained from the urban courtyard and from two WGW simulations made using the same 5-node layout with one also including an absorptive 'sky-node'.

materials). However, it was found that these simulations produced overly reverberant IRs due to the location's open nature not being compensated for. As such an extra, totally absorptive, node was added as a 'sky-node' to compensate for the open nature of the courtyard.

The 'sky-node' is implemented simply by adding a node at some arbitrary position and assigning it an α value of 0. In terms of Fig. 5 this in practice means all of the filter centered at that node will now include a coefficient such that all incoming samples are multiplied by zero.

Fig. 19 presents reverberation time for octave bands from 125 Hz to 16 kHz based on T30 for two WGW simulations compared with reverberation times obtained from the measured IR. In this figure the effect of adding a sky-node to the simulation can clearly be seen. Both WGW simulations in this case also had air absorption added using an analytical solution as presented in [49].

Fig. 19 shows general good agreement in reverberation time

results between the recorded and simulated IRs in octave bands from 500 Hz to 4 kHz but a larger deviation in the octave bands centered at 1 kHz and below. There remains considerable scope for further investigation into how best to model such a space, given the large number of possible node positions.

D. Computational Requirements

Table I shows the run time and memory required to run a WGW simulation of a forest environment with different numbers of nodes. For each simulation the source and receiver were positioned 10 m apart, and the nodes were positioned at random within a $10 \, \text{m}^2$ space between the source and receiver. Each simulation was computed to give 1s of audio output at a sampling rate of 48 kHz. From this table it can be seen there is a very large increase in memory usage with an increasing number of nodes. This exponential increase is due to the implementation of directionally dependent filtering at each node, which requires the implementation of N^2 filters at each of the N nodes—resulting in the number of filters required for implementation therefore increasing with N^3.

TABLE I
RUN TIME AND MEMORY REQUIRED FOR DIFFERENT NUMBERS OF NODES.

Nodes	Times (s)	Memory (MB)
5	4.35	5.65
10	9.58	18.32
15	39.65	672.10
20	155.89	5 508.98
25	358.38	27 350.03
30	667.23	102 404.16

V. CONCLUSION

This paper has presented the Waveguide Web, a new reverberator design for outdoor, or sparsely reflecting, environments, which offers an extension to De Sena's SDN reverberator to include accurate second-order reflections and directionally dependent filtering at each node. Following the presentation

of the WGW's design, several case studies were presented comparing WGW results with other examples. Firstly, a comparison was made with the SDN shoebox example as a validation of WGW operation. Secondly, a forest acoustic was modeled and compared with results from Spratt and Abel's Treeverb, which showed that the WGW produced more realistic results. This was further verified by considering the band gap absorption effect of a regular, grid-based, arrangement of trees. The results showed some agreement with prior work by Chobeau, indicating how acoustic attenuation due to the presence of such a regular arrangement of trees varies with tree/grid spacing. Spacings based on a higher filling fraction were also shown to increase global attenuation levels to some extent. The final case study was a comparison with impulse response measurements obtained from a semi-enclosed urban courtyard. Reverberation time results were in fairly good agreement following the incorporation of air absorption effects and the addition of a totally absorptive 'sky-node'.

The are several avenues for further research. The reflection/absorption filtering function for a node is well defined in the ideal specular case, and for the forest environment considered here. The boundary interactions observed in more general spaces, such as the urban courtyard example, are not so well defined in the context of this approach. The more formal use of acoustic bidirectional reflectance distribution functions to categorize reflecting nodes, as outlined in [2], may help in this regard. It would also be beneficial to implement analytical air absorption compensation directly as part of the WGW itself. The filtering currently used to represent a tree-node could also be extended to include filters of higher order, to better approximate Morse's solution to acoustic scattering from a rigid cylinder. It is also important to note that a limitation of the current forest model is that, like Treeverb, it does not include ground reflections or foliage. As such future work could also consider the addition of these aspects to the WGW by using results from [50].

This work represents an important step in the general development of reverberation algorithms more capable of modeling open acoustic scenes. Although this paper was in part inspired by the simulation of reverberant forest environments, the results can be applied in more general circumstances, with the WGW algorithm additionally offering improvements in terms of accuracy over other existing reverb algorithms. The WGW offers a new simulation tool for researchers interested in the perception of environmental acoustics and the associated effects that sound and our built or natural environment can have on human health and well-being.

ACKNOWLEDGEMENTS

REFERENCES

[1] V. Välimäki J. D. Parker, L. Savioja, J. O. Smith, and J. S. Abel, "Fifty years of artificial reverberation," *IEEE Trans Audio, Speech, and Lang. Process.*, vol. 20, no. 5, pp. 1421–1448, Jul. 2012.

[2] L. Savioja and U. P. Svensson, "Overview of geometrical room acoustic modeling techniques," *J. Acoust. Soc. Am.*, vol. 138, no. 2, pp. 708–730, Aug. 2015.

[3] A. Krokstad, S. Strom, and S. S., "Calculating the acoustical room response by the use of a ray tracing technique," *J. Sound Vibr.*, vol. 8, no. 1, pp. 118–125, Jan. 1968.

[4] J. B. Allen and D. A. Berkley, "Image method for efficiently simulating small-room acoustics," *J. Acoust. Soc. Amer.*, vol. 65, no. 4, pp. 943–950, Apr. 1979.

[5] J. Borish, "Extension of the image model to arbitrary polyhedra," *J. Acoust. Soc. Amer.*, vol. 75, no. 6, pp. 1827–1836, Jun. 1984.

[6] J. O. Smith, "A new approach to digital reverberation using closed waveguide networks," in *Proc. Int. Computer Music Conf.*, Vancouver, BC, Canada, Aug. 1985, pp. 47–53.

[7] P. Huang, M. Karjalainen, and J. Smith, "Digital waveguide networks for room response modeling and synthesis," in *Proc. Audio Eng. Soc. 118thth Conv.*, vol. 6394, Barcelona, Spain, May 2005, preprint no. 6394.

[8] J.-M. Jot and A. Chaigne, "Digital delay networks for designing artificial reverberators," in *Proc. Audio Eng. Soc. 90th Conv.*, Paris, France, Feb. 1991, preprint no. 3030.

[9] S. J. Schlecht and E. A. P. Habets, "Feedback delay networks: Echo density and mixing time," *IEEE/ACM Trans. Audio Speech Lang. Process.*, vol. 25, no. 2, pp. 374–383, Feb. 2017.

[10] S. J. Schlecht and E. A. Habets, "On lossless feedback delay networks," *IEEE Trans. Signal Process.*, vol. 65, no. 6, pp. 1554–1564, Mar. 2017.

[11] L. Savioja, T. Rinne, and T. Takala, "Simulation of room acoustics with a 3-D finite difference mesh," in *Proc. Int. Computer Music Conf.*, Aarhus, Denmark, Sept. 1994, pp. 463–466.

[12] K. Kowalczyk and M. van Walstijn, "Room acoustics simulation using 3-D compact explicit FDTD schemes," *IEEE Trans. Audio, Speech, Lang. Process.*, vol. 19, no. 1, pp. 34–46, Jan. 2011.

[13] S. Bilbao, "Modeling of complex geometries and boundary conditions in finite difference/finite volume time domain room acoustics simulation," *IEEE Trans. Audio Speech and Lang. Process.*, vol. 21, no. 7, pp. 1524–1533, Jul. 2013.

[14] S. Bilbao, B. Hamilton, J. Botts, and L. Savioja, "Finite volume time domain room acoustics simulation under general impedance boundary conditions," *IEEE/ACM Trans. Audio Speech and Lang. Process.*, vol. 24, no. 1, pp. 161–173, Jan. 2016.

[15] European Commission, "Directive 2002/49/EC of the European Parliament and the Council of 25 June 2002 relating to the assessment and management of environmental noise," *Official Journal of the European Communities, L*, vol. 189, no. 18.07, pp. 12–25, Jul. 2002.

[16] G. Watts, A. Miah, and R. Pheasant, "Tranquillity and soundscapes in urban green spaces predicted and actual assessments from a questionnaire survey," *Environment and Planning B: Planning and Design*, vol. 40, no. 1, pp. 170–181, Feb. 2013.

[17] W. Yang and J. Kang, "Acoustic comfort evaluation in urban open public spaces," *Applied Acoustics*, vol. 66, no. 2, pp. 211–229, Feb. 2005.

[18] E. De Sena, H. Hacihabiboglu, and Z. Cvetkovic, "Scattering delay network: An interactive reverberator for computer games," in *Proc. Audio Eng. Soc. 41st Int. Conf. Audio for Games*, London, UK, Feb 2011.

[19] F. M. Wiener, C. I. Malme, and C. M. Gogos, "Sound propagation in urban areas," *J. Acoust. Soc. Amer.*, vol. 37, no. 4, pp. 738–747, Apr. 1965.

[20] H. Sakai, S. Sato, and Y. Ando, "Orthogonal acoustical factors of sound fields in a forest compared with those in a concert hall," *J. Acoust. Soc. Amer.*, vol. 104, no. 3, pp. 1491–1497, Sep. 1998.

[21] M. Price, K. Attenborough, and N. Heap, "Sound attenuation through trees: measurements and models," *J. Acoust. Soc. Amer.*, vol. 84, no. 5, pp. 1836–1844, Nov. 1988.

[22] H. Sakai, S. Shibata, and Y. Ando, "Orthogonal acoustical factors of a sound field in a bamboo forest," *J. Acoust. Soc. Amer.*, vol. 109, no. 6, pp. 2824–2830, Jun. 2001.

[23] T. Lokki, A. Southern, S. Siltanen, and L. Savioja, "Acoustics of Epidaurus—Studies with room acoustics modelling methods," *Acta Acust. united Ac.*, vol. 99, no. 1, pp. 40–47, Jan. 2013.

[24] M. Lopez, S. Pauletto, and G. Kearney, "The application of impulse response measurement techniques to the study of the acoustics of Stonegate, a performance space used in medieval English drama," *Acta Acust. united Ac.*, vol. 99, no. 1, pp. 98–109, Jan. 2013.

[25] J. Kang, "Numerical modeling of the sound fields in urban squares," *J. Acoust. Soc. Amer.*, vol. 117, no. 6, pp. 3695–3706, Jun. 2005.

[26] R. E. Collecchia, J. S. Abel, S. Coffin, E. Callery, Y. H. Yeh, K. Spratt, and J. O. Smith, III, "On the acoustics of alleyways," in *Proc. Audio Eng. Soc. 137th Conv.*, Los Angeles, USA, Oct. 2014.

[27] J. Stienen and M. Vorländer, "Auralization of urban environments—Concepts towards new applications," in *Proc. EuroNoise 2015*, Maastricht, The Netherlands, Jun. 2015.

[28] F. Stevens and D. T. Murphy, "Spatial impulse response measurement in an urban environment," in *Proc. Audio Eng. Soc. 55th Int. Conf. Spatial Audio*, Helsinki, Finland, Aug. 2014.

[29] ——, "Acoustic source localisation in an urban environment using early reflection information," in *Proc. EuroNoise 2015*, Maastricht, The Netherlands, Jun. 2015.

[30] R. Pieren and J. M. Wunderly, "A model to predict sound reflections from cliffs," *Acta Acust. united Ac.*, vol. 97, no. 2, pp. 243–253, Mar. 2011.

[31] S. Shelley, D. T. Murphy, and A. Chadwick, "B-format acoustic impulse response measurement and analysis in the forest at Koli national park, Finland," in *Proc. 16th Int. Conf. Digital Audio Effects (DAFx-13)*, Maynooth, Ireland, Sept. 2013, pp. 351–355.

[32] S. Harriet and D. T. Murphy, "Auralisation of an urban soundscape," *Acta Acustica united with Acustica*, vol. 101, no. 4, pp. 798–810, jul 2015.

[33] K. Spratt and J. S. Abel, "A digital reverberator modeled after the scattering of acoustic waves by trees in a forest," in *Proc. Audio Eng. Soc. 125th Conv.*, San Francisco, CA, Oct. 2008.

[34] E. D. Sena, H. Hacihabiboglu, Z. Cvetkovic, and J. O. Smith, "Efficient synthesis of room acoustics via scattering delay networks," *IEEE/ACM Trans. Audio, Speech, and Language Process.*, vol. 23, no. 9, pp. 1478–1492, Sept. 2015.

[35] S. Van Duyne and J. O. Smith, "The 2-D digital waveguide mesh," in *Proc. IEEE Workshop Appl. Signal Process. Audio Acoust. (WASPAA)*, New Paltz, NY,USA, Oct. 1993, pp. 177–180.

[36] F. Fontana and D. Rocchesso, "Signal-theoretic characterization of waveguide mesh geometries for models of two-dimensional wave propagation in elastic media," *IEEE Trans. Speech and Audio Process.*, vol. 9, no. 2, pp. 152–161, Feb 2001.

[37] D. T. Murphy, A. Kelloniemi, J. Mullen, and S. Shelley, "Acoustic modeling using the digital waveguide mesh," *IEEE Signal Process. Mag.*, vol. 24, no. 2, pp. 55–66, Mar. 2007.

[38] B. Hamilton, "Sampling and reconstruction on a diamond grid and the tetrahedral digital waveguide mesh," *IEEE Signal Process. Lett.*, vol. 10, no. 20, pp. 925–928, Oct. 2013.

[39] P. Morse, *Vibration and sound.* McGraw-Hill New York, 1948.

[40] P. Chobeau, "Modeling of sound propagation in forests using the transmission line matrix method," Ph.D. dissertation, Université du Maine, Le Mans, France, Nov. 2014.

[41] T. Wiens, "Forest reverb generator – file exchange – MATLAB central," Jul. 2008, [Accessed: 03-11-2015]. [Online]. Available: http://www.mathworks.com/matlabcentral/fileexchange/20764-forest-reverb-generator

[42] F. Stevens. (2017) Waveguide web example audio. [Online]. Available: http://www.openairlib.net/auralizationdb/content/waveguide-web-example-audio

[43] ISO 3382-1, "Acoustics, measurement of room acoustic parameters. part 1: Performance spaces,," *The International Organization for Standardization*, 2009.

[44] ISO 3382-2, "Acoustics, measurement of room acoustic parameters. part 2: Reverberation time in ordinary rooms,," *The International Organization for Standardization*, 2009.

[45] Z. Meng, F. Zhao, and M. He, "The just noticeable difference of noise length and reverberation perception," in *Proc. Int. Symp. Communications and Info. Technologies*, Bangkok, Thailand, Oct. 2006, pp. 418–421.

[46] W. Robertson and J. Rudy III, "Measurement of acoustic stop bands in two-dimensional periodic scattering arrays," *J. Acoust. Soc. Amer.*, vol. 104, no. 2, pp. 694–699, Aug. 1998.

[47] S. Harriet, "Application of auralisation and soundscape methodologies to environmental noise," Ph.D. dissertation, University of York, York, UK, 2013.

[48] T. Miyashita, "Sonic crystals and sonic wave-guides," *Measurement Science and Technology*, vol. 16, no. 5, p. R47, Apr. 2005.

[49] H. Bass, H.-J. Bauer, and L. Evans, "Atmospheric absorption of sound: Analytical expressions," *J. Acoust. Soc. Amer.*, vol. 52, no. 3B, pp. 821–825, Sep. 1972.

[50] K. Attenborough, "Ground parameter information for propagation modeling," *J. Acoust. Soc. Amer.*, vol. 92, no. 1, pp. 418–427, Jul. 1992.

PLACE PHOTO HERE

Francis Stevens received the M.Eng. (Hons.) degree in electronic engineering with music technology systems from the University of York, UK, in 2014. He is currently a PhD candidate in the AudioLab based in the Department of Electronic Engineering, University of York, UK. His research interests include environmental sound measurement, modeling, and evaluation. He is a student member of the Audio Engineering Society.

PLACE PHOTO HERE

Damian T. Murphy received the B.Sc. (Hons.) degree in mathematics, the M.Sc. degree in music technology, and the D.Phil. degree in music technology, all from the University of York, UK, in 1993, 1995, and 2000, respectively. He is a Reader in the AudioLab based in the Department of Electronic Engineering, University of York, where he has worked since 2000 and is a Visiting Lecturer in the Department of Speech, Music, and Hearing, KTH, Sweden and has held visiting researcher positions at a number of universities internationally. His research interests include acoustic modeling and spatial audio. He is a member of the Audio Engineering Society.

PLACE PHOTO HERE

Lauri Savioja (M'02–SM'11) works as a Professor and the Head of Department for the Department of Computer Science, Aalto University School of Science, Espoo, Finland. He received the degree of Doctor of Science in Technology in 1999 from the Department of Computer Science, Helsinki University of Technology. His research interests include room acoustics, virtual reality, and auditory displays. He is a Fellow of the Audio Engineering Society (AES), and a Member of the Association for Computing Machinery (ACM), and the Acoustical Society of Finland.

PLACE PHOTO HERE

Vesa Välimäki (S'90–M'92–SM'99–F'15) received the M.Sc. in Technology and the Doctor of Science in Technology degrees in electrical engineering from the Helsinki University of Technology (TKK), Espoo, Finland, in 1992 and 1995, respectively.

He was a Postdoctoral Research Fellow at the University of Westminster, London, UK, in 1996. In 1997–2001, he was a Senior Assistant at TKK. In 2001–2002, he was a Professor of signal processing at the Pori unit of the Tampere University of Technology, Pori, Finland. In 2006–2007, he was the Head of the TKK Laboratory of Acoustics and Audio Signal Processing. In 2008–2009, he was a Visiting Scholar at Stanford University. He is currently a Professor of audio signal processing and the Vice Dean for Research in the School of Electrical Engineering, Aalto University, Espoo, Finland. His research interests include artificial reverberation, headset audio, nonlinear audio processing, and musical instruments.

Prof. Välimäki is a Fellow of the Audio Engineering Society and a Life Member of the Acoustical Society of Finland. In 2007–2013 he was a Member of the Audio and Acoustic Signal Processing Technical Committee of the IEEE Signal Processing Society and is currently an Associate Member. He is a Founding Member of the EURASIP Special Area Team in acoustic, sound and music signal processing (2015 to present). He served as an Associate Editor of the IEEE SIGNAL PROCESSING LETTERS in 2005–2009 and of the IEEE TRANSACTIONS ON AUDIO, SPEECH AND LANGUAGE PROCESSING in 2007–2011. He was in the Editorial Board of the *Research Letters in Signal Processing*, of the *Journal of Electrical and Computer Engineering*, and of *The Scientific World Journal*. He was the Lead Guest Editor of a special issue of the IEEE SIGNAL PROCESSING MAGAZINE in 2007 and of a special issue of the IEEE TRANSACTIONS ON AUDIO, SPEECH AND LANGUAGE PROCESSING in 2010. In 2015, he was a Guest Editor of the special issue of the IEEE SIGNAL PROCESSING MAGAZINE on signal processing techniques for assisted listening. In 2016, he was the Lead Guest Editor of the special issue of *Applied Sciences* on audio signal processing. Since 2015 he has been a Senior Area Editor of the IEEE/ACM TRANSACTIONS ON AUDIO, SPEECH AND LANGUAGE PROCESSING. In 2008, he was the Chair of DAFX-08, the 11th International Conference on Digital Audio Effects. He is the Chair of the Sound and Music Computing Conference SMC-17, which is held in Espoo, Finland in July 2017.